Research Article | Submit Manuscript

Turkish Journal of Materials

Exploration of impact of Cr-doping on physical and optical properties of CdS thin films in hybrid photovoltaic cells

Salih Yılmaz[1,*], Ahmet Ünverdi[2], Murat Tomakin[3], Melek Altay[1], İsmail Polat[4], Emin Bacaksız[5]

[1]Department of Materials Engineering, Faculty of Engineering, Adana Alparslan Türkeş Science and Technology University, Adana, Turkey

[2]Nanotechnology and Engineering Sciences, Graduate School of Natural and Applied Sciences, Adana Alparslan Türkeş Science and Technology University, Adana, Turkey

[3]Department of Physics, Faculty of Arts and Sciences, Recep Tayyip Erdogan University, Rize, Turkey

[4]Department of Energy Systems Engineering, Faculty of Technology, Karadeniz Technical University, Trabzon, Turkey

[5]Department of Physics, Faculty of Sciences, Karadeniz Technical University, Trabzon, Turkey

Received: 27 May 2020; Accepted: 12 August 2020; Published: 31 August 2020

Turk. J. Mater. Vol: 5 No: 1 Page: 1-9 (2020) ISSN: 2636-8668

SLOI: http://www.sloi.org/sloi-name-of-this-article

*Correspondence E-mail: slh_yilmaz@yahoo.com.tr (Salih YILMAZ)

ABSTRACT This paper searches for varying Cr-doping on both physical, optical properties of CdS thin films and their photovoltaic applications. CdS:Cr thin films with Cr atoms from 0 to 8% are produced by chemical bath deposition. X-ray diffraction conclusion shows that all samples grow in cubic structure and Cr-doping leads to formation of nanocrystalline CdS structure. Scanning electron microscopy data demonstrates that a reduction in grain size is obtained by Cr-doping. P3HT layer is almost uniformly coated on N3-modified CdS or CdS:Cr surfaces. 2% and 8% Cr-doped CdS thin films exhibit better transparency than that of CdS sample in the visible region. Band gap values increase from 2.98 eV to 3.36 eV when Cr-doping concentration alters from 0% to 4%, which could be probably due to the quantum confinement effect. Absorbance of CdS-based device decreases after Cr-doping. Photoluminescence curves illustrate that peak intensity increases upon Cr-doping that is ascribed to radiative recombination induced by Cr atoms. Photoluminescence data displays that Cr-doped CdS-based devices have higher peak intensity than that of CdS. It is obtained from photovoltaic measurements that CdS-based hybrid solar cell demonstrates a power conversion efficiency of 0.296%.

Keywords: CdS:Cr thin films; chemical bath deposition; physical properties; optical properties; hybrid photovoltaic cell.

Cite this article: S. Yılmaz, A. Ünverdi, M. Tomakin, M. Altay, İ. Polat, E. Bacaksız. Exploration of impact of Cr-doping on physical and optical properties of CdS thin films in hybrid photovoltaic cells. Turk. J. Mater. 5(1) (2020) 1-9.

1. INTRODUCTION

In recent years, demand on renewable energy sources has increased significantly after increment of global warming. Our atmosphere is getting overwhelmed with carbon dioxide (CO_2) and other global warming emissions due to the human activity. The heat coming from sun is trapped because of these gases since they prevent the heat going back to space and this causes significant impacts such as more frequently and stronger storms, extinction, rising sea level and drought. However, the impact of renewable energy sources on global warming emissions is quite low. Therefore, studies have increased on solar cells - one of the most beneficial and clean renewable energy sources - operating as semiconductors, which is a

photovoltaic system that directly converts the solar rays into electrical current.

Solar cells have been considered within three main areas according to types of materials utilized. Those are inorganic-inorganic, organic-organic and hybrid solar cells. The hybrid solar cells have been commonly studied due to the combination of both advantages of inorganic and organic materials. Inorganic and organic materials are used as electron acceptor and donor in hybrid solar cells, respectively [1, 2].

As an inorganic material, CdS is a significant n-type semiconductor of II-VI group elements and has great optical and electrical properties such as a direct band gap (2.42 eV at RT) and an excellent photosensitivity besides having high stability, low resistivity and remarkable electron mobility. These properties make CdS an important material in the field of LEDs, sensors and solar cells [3-5]. P3HT, on the other hand, is one of the most commonly used organic semiconductor material due to its characteristics including excellent hole mobility, notable surface adhesion and high thermal stability [5].

The synthesis of CdS has been carried out via different methods such as hydrothermal method [6], electrodeposition [7], spray pyrolysis [8] and chemical bath deposition method (CBD) [9]. CBD is one of well-established thin film deposition techniques. In this method, thin films deposition is carried out from aqueous solutions at low temperatures. N3 dye was used for the interfacial engineering, which led to a better light absorbance owing to the formation of better surface contact at CdS/P3HT interface [5]. In other words, dye modification was utilized to enhance the performance of hybrid solar cell. Another way to tune not only the physical, optical properties of CdS materials but also the solar cells characteristics is doping with an appropriate material. Chromium (Cr) is chosen as doping material because CdS including Cr atoms plays an important role in the optoelectronic area [10]. Furthermore, band gap engineering could be also achieved by Cr-doping via controlling the crystalline size of CdS. That is, the decrease of crystalline size below the Bohr exciton radius (about 5.8 nm for bulk CdS) causes quantum confinement of electron-hole, giving rise to a widening of band gap of CdS material [11, 12].

It has been noticed from the literature survey that the population of experimental studies investigating structural, morphological, optical and magnetic properties of Cr-doped CdS samples is limited. Some of them can be discussed as follows: Kumar and co-workers prepared CdS nanoparticles by a co-precipitation route. They found a decrease in the intensity of main XRD peaks of CdS samples upon Cr-doping [13]. A study of Cr-doped CdS quantum dots grown by lyothermal technique was reported by Srivastava et al., demonstrating the presence of the room temperature ferromagnetism for both undoped and Cr-doped CdS samples [14]. Thambidurai and co-workers prepared CdS nanoparticles by chemical precipitation method and investigated the structural and optical properties of the samples. They obtained a blue shift in the band gap of CdS samples after Cr-doping [12]. On the other hand, according to our best of knowledge, there is no reported work dealing with the physical, optical and photovoltaic properties of Cr-doped CdS-based hybrid solar cell in the literature although Cr-doped CdS-based dye sensitized solar cells (DSSCs) was published by Horoz et al. In that study, Cr-doped CdS quantum dots were produced by the co-precipitation method and the effects of Cr-doping on some physical properties and performance of the DSSCs were researched [15].

In this paper, examinations of how chromium concentration affects physical and optical properties of CdS thin films as well as photovoltaic characteristics of solar cells were studied by changing Cr-doping concentration from 0% to 8% with a rise of 2%. To fabricate the hybrid solar cells, ITO covered glass pieces were utilized as substrates. CdS thin films were prepared by CBD technique on ITO slides. Then, N3 dye (interfacial modifier) and P3HT were spin coated, respectively, on the surface of CdS and CdS:Cr thin films. Ag paste was deposited on top of the pristine (ITO/CdS/ N3/P3HT) and Cr-doped CdS-based (ITO/CdS:Cr/N3/P3HT) heterostructures to finalize the hybrid solar cells.

2. EXPERIMENTAL

Indium tin oxide (ITO) coated glass substrates were divided into eight pieces with a surface area of 1.25×1.0 cm^2 per piece through a diamond insert. To perform cleaning process of substrates; sulfuric acid, distilled water and ethanol were used, respectively, in an ultrasonic bath as 10 minutes for each and finally the substrates were dried by flowing of nitrogen gas. 0.02 M of cadmium chloride ($CdCl_2$), 0.05 M of thiourea (CH_4N_2S) and 0.05 M of ammonium chloride (NH_4Cl) materials were utilized in the preparation of CdS solution. Three different beakers were taken and 20 ml of distilled water was filled by each and desired weights of cadmium chloride, thiourea and ammonium chloride were added separately into each beaker. All the beakers were bathed ultrasonically for 2 minutes to obtain homogenous solution and thus, total of 60 ml solution was attained. In addition, 15 ml of ammonia solution (NH_4OH) was added into the prepared solution to form 75 ml of CdS solution. On the other hand, while the molarities of thiourea, ammonia solution and ammonium chloride were kept the same, suitable amounts of cadmium chloride and chromium chloride ($CrCl_3.6H_2O$) were used to produce CdS:Cr solutions including Cr doping of 2%, 4%, 6% and 8%. Subsequently, the solutions were poured into teflon apparatus and then it was placed on a hotplate while the teflon was kept constant in the middle of a half-filled beaker with water. Two thermometers were placed in each solution to control both temperatures constantly. Then, the solutions were heated up to 75°C in a few hours and ensured to be kept constant at that temperature for 15 minutes to grow CdS and CdS:Cr thin films.

Dye coating process was carried out via a spin coater using a 50 ml of N3 dye solution that was prepared by merging suitable amount of N3 dye in absolute ethanol. The samples with and without (Cr) doping were waited in this solution for 24 hours. After immersing process, it was noticed that dye coating on the surface of CdS thin films weren't enough and therefore, more N3 dye was coated on the surface of specimens through a spin-coater. During spin-coating process, the rotational speed

of the device was set at 1000 rpm while the progress was applied as 6 times for 1 minute. Similarly, 20 mg/ml commercial P3HT material was dissolved in 2 ml of chlorobenzene and then the prepared solution was spin-coated on the surface of the samples modified by N3 dye. In this process, P3HT solution was applied 5 times on the surface of each sample. To finalize CdS-based hybrid solar cells, alloy of Ga-In was employed as back contact while Ag paste with a contact area of 0.008 cm^2 was applied as a front contact on P3HT layers.

CdS, 2%, 4%, 6% and 8% Cr-doped CdS samples were coded as C0, C2, C4, C6 and C8, respectively. On the other hand, ITO/CdS/N3 dye/P3HT/Ag, ITO/CdS:Cr (2%)/N3 dye/P3HT/Ag, ITO/CdS:Cr (4%)/N3 dye/P3HT/Ag, ITO/CdS:Cr (6%)/N3 dye/P3HT/Ag and ITO/CdS:Ni (8%)/N3 dye/P3HT/Ag hybrid solar cells were labeled as C0-Device, C2-Device, C4-Device, C6-Device and C8-Device, respectively. Structural characterization of CdS and Cr-doped CdS thin films was carried out by X-ray diffraction measurement (Rigaku SmartLab Unit) with a measurement step of 0.02° between 20° and 60° with a Cu Kα radiation. The surface morphology of CdS and Cr-doped CdS thin films as well as their devices was performed through scanning electron microscopy (SEM, JEOL JSM 6610). To analyze the elemental ingredient (EDS) of CdS and Cr-doped CdS thin films, Energy dispersive X-ray spectroscopy (EDS, Oxford Instruments) attached to SEM was utilized. The transparency of the films was measured in the wavelength range of 400-1000 nm via UV-VIS spectrophotometer (SpectraMax M5). A laser with an excitation wavelength of 532 nm was carried out for PL measurements of CdS-based devices through a SpectraMax M5 instrument whereas room temperature photoluminescence (RTPL) data was taken by an excitation wavelength of 280 nm for CdS and Cr-doped CdS samples via the same device. The current density-voltage (J-V) characteristics of the hybrid solar cells were obtained via a source meter (Keithley 2410) with a 93 mW/cm^2 power output under a solar simulator (AM 1.5D illumination).

3. RESULTS AND DISCUSSION

Figure 1(a)-(e) represent the XRD data of C0, C2, C4, C6 and C8 samples. It is noted from Figure 1(a) that CdS thin films grow in polycrystalline nature with (111), (200) and (311) planes indexed to hawleyite (cubic) CdS structure (JCPDS card no: 75-1546). The preferred orientation of CdS is along (111) plane. In addition to peaks of cubic CdS structure, some peaks belonging to ITO-covered glass substrates appear and it can be seen that these peaks dominate all the patterns. There is no variation in the cubic crystal structure of CdS thin films with the addition of Cr-atoms and it is also worth saying that the peak intensities of CdS reduce remarkably, which means that the crystal qualities of C2, C4, C6 and C8 samples get worse. A broadening appeared in the (111) peak for the samples containing Cr atoms means the creation of nanocrystalline CdS structure as indicated in Figure 1(b)-(d). Kumar and co-workers obtained a similar data for Cr-doped CdS nanoparticles grown by a chemical route [13]. On the other hand, the (220) and (311) peaks almost disappear for the samples containing Cr-atoms. Except for CdS and ITO peaks, there is no metallic Cr or its compound such as Cr_2S_3 in the pattern, which is the indication of successful incorporation of Cr^{3+} atoms into CdS structure. It is tabulated that the lattice parameter (*a*) of C0 sample is determined to be 0.578 nm and it seems a fluctuation in this value for C2, C4 and C6 samples and it comes back the value of that of CdS one, implying that Cr-doping doesn't change too much the lattice parameter of CdS. Scherrer relation is used to determine the crystalline sizes (*D*) of the samples and all the data are listed in Table 1. It is observed that CdS possesses a *D* of 17.4 nm. After doping of Cr for various amounts (C2, C4, C6 and C8), CdS thin films exhibit smaller *D* values, meaning that Cr-doping causes a reduction in the crystalline size of CdS thin films. Particularly, C2 and C4 samples exhibit very small values compared to that of CdS one, which is an indication of the formation of nanocrystalline structure [5]. This could result from the change in the nucleation mechanism of CdS due to addition of Cr atoms into host structure [16].

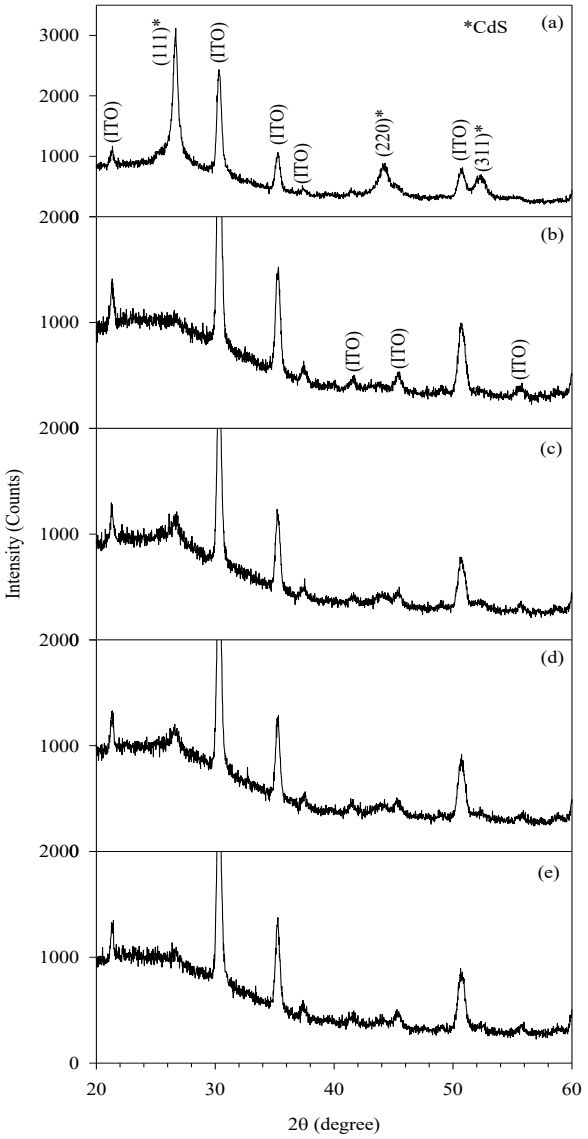

Fig. 1. XRD data of (a) C0, (b) C2, (c) C4, (d) C6 and (e) C8 samples.

Figure 2(a)-(e) display the top view image of C0, C2, C4, C6 and C8 samples. C0 sample possesses grains with spherical shape and their distribution is almost uniform on the surface of ITO-covered glass substrates. The average value of grain size is nearly 100 nm while the surface of sample is a compact and dense without fracture. After doping of 2% Cr (Figure 2(b)), a fundamental morphological change is observed. That is, smaller grains are formed and some aggregates that are undefined in shape appear above these grains. The density of these uncertain shaped aggregates isn't too many and they accumulate at certain places on the surface. Compared to that of C0 sample, the grain size of C2 specimen decreases remarkably. When Cr-doping concentration is increased to 4% (C4) it is clearly seen that the grains, which are too small to be seen, take place besides the formation of very smooth surface.

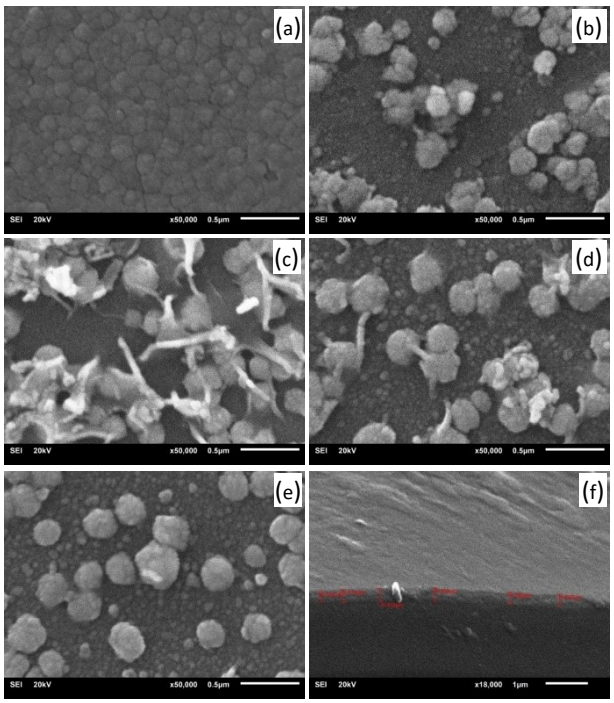

Fig. 2. Top view SEM images of (a) C0, (b) C2, (c) C4, (d) C6 and (e) C8 samples and (f) displays 60° tilted picture of C8 specimen.

However, some aggregates are also observed above the small grains. A similar decrease in the particle size was also reported by Thambidurai and co-workers for CdS:Cr nanoparticles synthesized by a precipitation method with addition of Cr atoms in CdS [12]. On the other hand, C6 and C8 samples (Figure 2(d)-(e)) have slightly bigger grains in size with respect to those of C2 and C4 samples. The grain shape is spherical and some aggregates are formed above the small grains, which is almost uniform in size. Except for that of CdS, all Cr-doped CdS thin films exhibit some aggregates on the surface, which is probably due to the merging of smaller grains to form the bigger ones caused by Cr-doping as a result of reorganization of CdS structure after incorporation of Cr atoms in CdS structure. It can be also stated that all Cr-doped CdS samples possess smaller grains than that of CdS one, which is in good agreement with the reduction of crystalline sizes of CdS thin films upon Cr-doping as discussed above. 60° tilted view of C8 specimen is displayed in Figure 2(f), implying that C8 sample exhibits an average thickness of 290 nm. In overall, it can be declared that Cr-doped CdS thin films present thin thickness, which could demonstrate the presence of nanocrystalline structure.

Plain view images of C0-Device, C2-Device, C4-Device, C6-Device and C8-Device are illustrated in Figure 3(a)-(e), respectively. Figure 3(a) shows that the coverage of P3HT layer is nonuniform and some distortions are observed on the surface of CdS thin films. For the heterostructures of C2-Device, C4-Device and C8-Device, P3HT coating on various Cr-doped CdS thin films seems smooth, dense, and compact without any fracture, meaning that better surface morphology is reached. However, as seen Figure 3(c), C4-Device exhibits totally different morphology. That is, surface coverage of P3HT is good enough while higher roughness is found compared with the others. This is because bottom layer grows in the grainy-shaped morphology. The 60° tilted photography of C8-Device is displayed in Figure 3(f), stating that the thickness of P3HT layer is almost 159 nm.

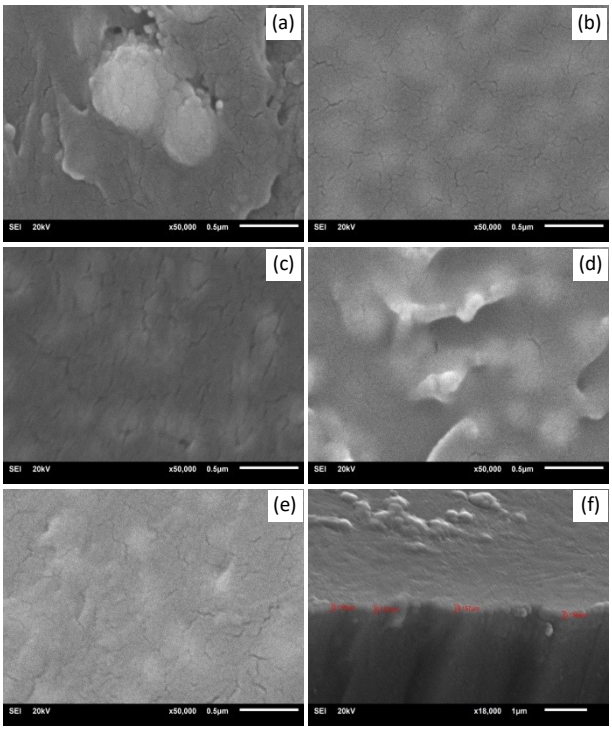

Fig. 3. Plain view SEM pictures of (a) C0-Device, (b) C2-Device, (c) C4-Device, (d) C6-Device, (e) C8-Device and (f) shows 60° tilted image of C8-Device.

EDS survey spectra of C0, C2, C4, C6 and C8 samples are displayed in Figure 4(a)-(e), respectively, and the insets of all the figures show the measured atomic concentrations of the samples. Figure 4(a) shows that C0 sample solely consists of Cd and S elements. After Cr-dopings with various amounts, EDS survey spectrum exhibits Cr peak besides Cd and S peaks, approving the successful incorporation of Cr atoms into CdS. It is observed from the insets of C2, C4, C6 and C8 samples that the measured atomic concentrations of Cr atoms are slightly higher than those of nominal ones because of nonhomogeneous distribution of Cr atoms in CdS structure. It is also seen that as the nominal Cr

density increase in CdS thin films, the actual one rises as well. It is found that Cd/S ratio for C0 sample is nearly 1.01, suggesting a stoichiometric formation of CdS thin films. This ratio fluctuates for intermediate Cr-doping amounts and then approaches approximately 0.95 for C8 sample, meaning that a deviation in the stoichiometry is obtained. This results in the creation of more intrinsic defected CdS structure, which will be handled in PL data.

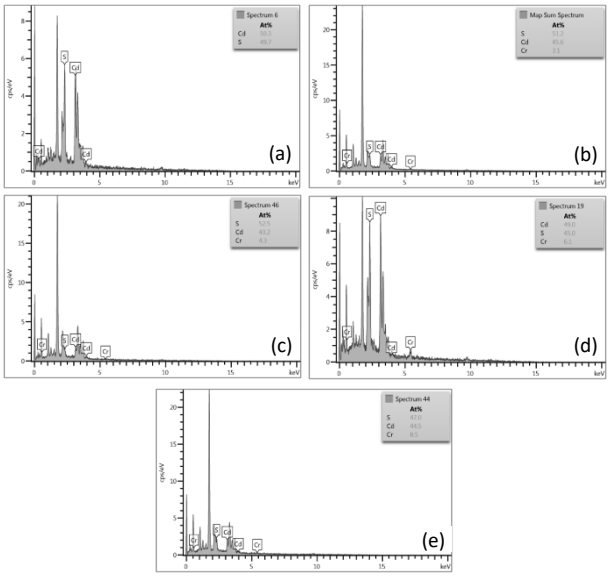

Fig. 4. EDS survey spectra of (a) C0, (b) C2, (c) C4, (d) C6 and (e) C8 samples.

Transmittance results of C0, C2, C4, C6 and C8 samples are demonstrated in Figure 5. It can be seen that C0 sample has an increasing transparency in the visible region and then it has a transmission of 90% at almost 850 nm. After Cr-doping with various amounts, the shape of the transmission curve is the same. However, the transmissions for C2 and C8 samples throughout the spectrum are higher than that of C0 one.

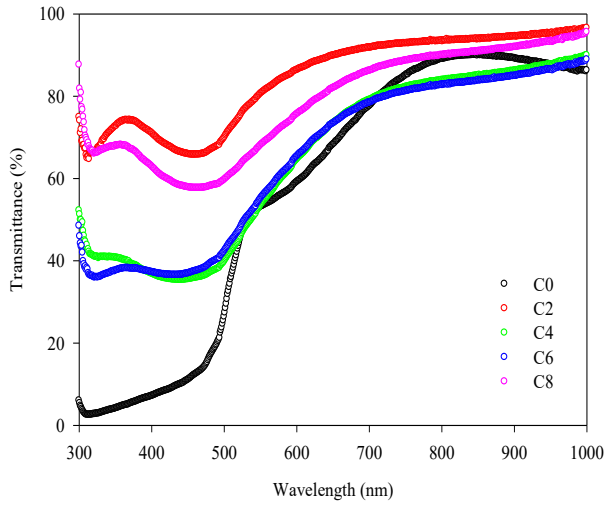

Fig. 5. Transmittance curves of C0, C2, C4, C6 and C8 samples.

In other words, more transparent CdS thin films are formed, which are very important for solar cell applications since they can be efficiently used as a window layer. On the other hand, an increasing trend in transmission plots for the samples including Cr atoms is observed with the rise of wavelength up to 1000 nm. However, C4 and C6 samples display lower transmittance values than that of C0 in the wavelength interval of 700-900 nm, proposing a decline in the transparency whereas remaining transmittance spectra for these samples are also higher. The reason for the decline could be ascribed to the creation of the morphological distortion created by 4% and 6% Cr-dopings as seen in Figure 2(c)-(d). The other reason for the decline is most probably due to the reduction in grain size, saying that Cr-doping triggers a decline in the grain size, which leads to more grain boundaries and hence more grain boundary scattering. The absorption edge of C0 sample exhibits quite steep rise, implying that it has a better crystal quality. Yet, Cr-doped CdS thin films show an inclined absorption edge which means that a degradation is obtained in the crystal degree of samples, which is in good agreement with XRD results. It is also observed that the absorption edge shifts to the shorter wavelengths with incorporation of Cr atoms into CdS structure.

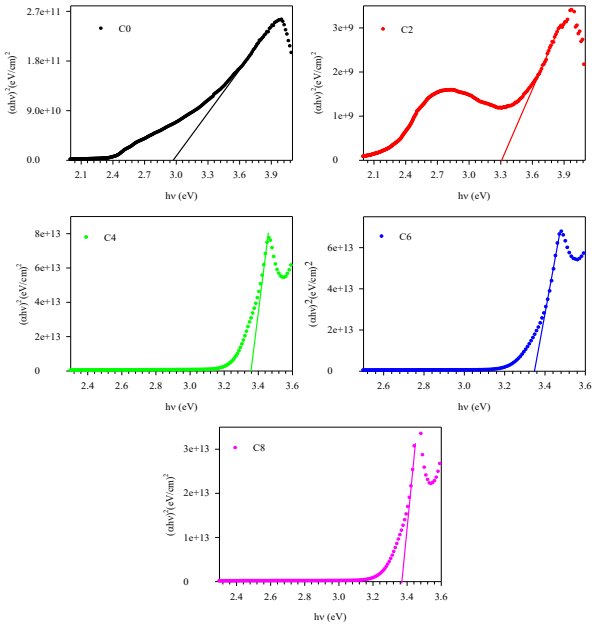

Fig. 6. Tauc's plots of C0, C2, C4, C6 and C8 samples.

Forbidden band gaps of C0, C2, C4, C6 and C8 samples are determined employing Tauc's expression and the conclusions are represented in Figure 6. It is appeared that C0 sample possesses a band gap value of 2.98 eV, which is bigger than that of bulk one (2.42 eV at 300 K). This difference in the band gap is most probably due to the quantum size effect, which is exhibited by the samples with a lower crystalline size [6]. Sarma et al. reported an analogous band gap of 2.90 for undoped CdS quantum dots prepared by co-precipitation technique [11]. After 2% Cr-doping (C2), the band gap value of CdS thin films substantially increases to 3.30 eV and further increase of Cr-doping concentration to 4% (C4) gives rise to more rising in the band gap as 3.36 eV. Compared to the band gap of C0 sample, this gradual enhancement in the band gap could possibly originate from the strong quantum confinement

effect, which occurs as the crystalline size reduces below the Bohr exciton radius (nearly 5.8 nm for CdS) [14]. As can be seen in Table 1, the crystalline size decreases importantly after Cr-doping of 2% and 4% and these values are lower than that of Bohr exciton radius for CdS. Therefore, it can be pronounced that band gap enlargement is originating from the strong quantum confinement effect. On the other hand, this band gap value of CdS thin films doesn't change significantly for 6% Cr (C6) and 8% Cr (C8) dopings, which could imply that further increase of Cr atoms in CdS structure doesn't cause more band gap increment as given in Table 1. The formation of CdS thin films with large band gaps is essential because they can be effectively utilized in solar cells as a window layer.

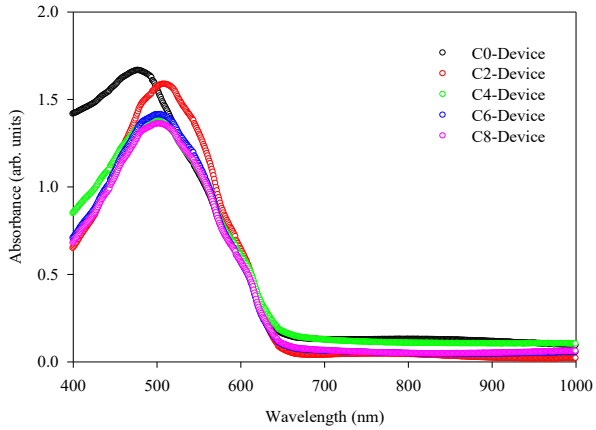

Fig. 7. Absorbance data of C0-Device, C2-Device, C4-Device, C6-Device and C8-Device heterostructures.

Absorption plots of C0-Device, C2-Device, C4-Device, C6-Device and C8-Device are indicated in Figure 7. It is obtained that C0-Device has a wide absorbance in the wavelength interval of 400-650 nm with a maximum at 478 nm, which could be owing to vibronic transition of P3HT polymer [17]. Although the shapes of the peaks seem very similar to all the devices, their peak maxima move toward longer wavelength compared to that of C0-Device, meaning that a red shifting in the absorption spectra appears. Sharma and co-workers and Srivastava and co-workers reported that the main absorption peaks shifted to the longer wavelengths as Cr atoms were doped in CdS quantum dots [11, 14].

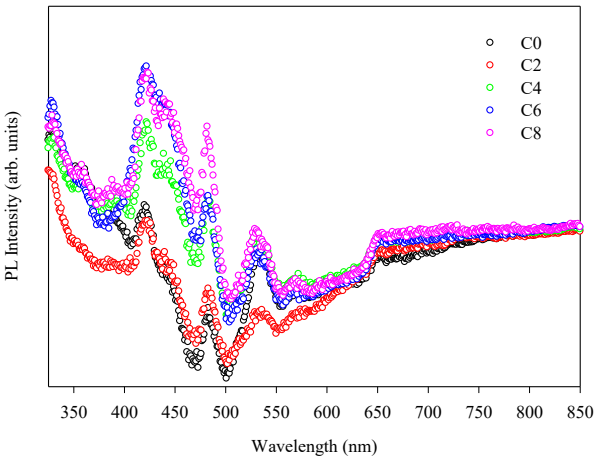

Fig. 8. RTPL plots of C0, C2, C4, C6 and C8 samples.

The absorption peak intensities of devices including Cr atoms are lower than that of C0-Device, meaning that a deterioration in the N3-dye absorption on CdS surface was acquired after Cr-doping. This reduction in the absorbance leads to less compatible CdS/P3HT interface.

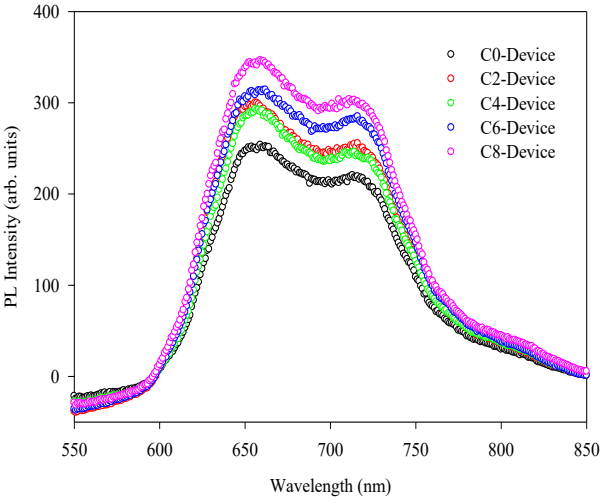

Fig. 9. RTPL data of C0-Device, C2-Device, C4-Device, C6-Device and C8-Device heterostructures.

RTPL plots of C0, C2, C4, C6 and C8 samples are shown in Figure 8. It can be stated that CdS materials with a stoichiometric deviation from unity have point defects including V_{Cd}, I_{Cd}, V_S, I_S and/or their complexes. It is noticeable that four main peaks are observed in the spectrum for C0 sample which is centered at 420 nm, 483 nm, 533 nm and 649 nm. Band edge emission of CdS thin films results from the first peak that is due to the recombination of electron-hole pairs, which is consistent with Tauc's analysis result. The second peak exhibiting asymmetric shape with a shoulder at 444 nm is associated with host CdS matrix [18].

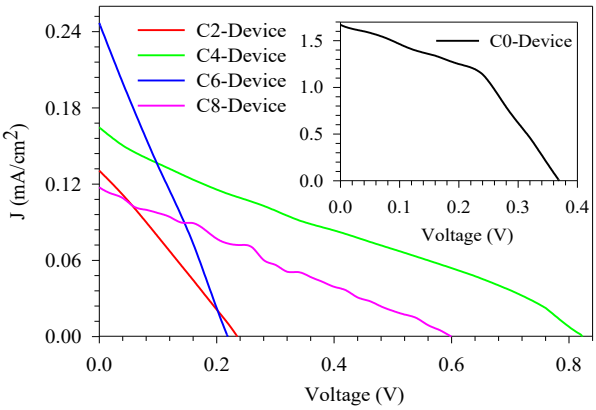

Fig. 10. J-V curves of C2, C4, C6 and C8 devices and inset indicates J-V curve of C0-Device for the comparison.

On the other hand, Mercy and co-workers attributed the shoulder peak to the recombination of band edge [19]. Third peak is most probably due to the V_S defects [20] while fourth one is ascribed to the V_{Cd} defects triggered by surface defects [21]. PL peak intensity gradually ascends with the increment of Cr atoms in CdS thin films as illustrated in Figure 8, implying the creation of more defected CdS samples, which is also in good agreement with EDS conclusions. The reason for the enhancement in the PL peak intensity could be imputed to the radiative recombination phenomenon induced by Cr-doping. Analogous conclusion was also obtained by Yılmaz et al. for ZnO:Cr microrods synthesized through spray pyrolysis route [22].

Table 1. Lattice constants and crystalline sizes of C0, C2, C4, C6 and C8 samples.

Sample	Lattice constant (*a*) (nm)	Crystalline size (*D*) (nm)
C0	0.578	17.4
C2	0.578	2.4
C4	0.581	3.1
C6	0.580	8.9
C8	0.578	12.2

RTPL conclusions of C0-Device, C2-Device, C4-Device, C6-Device and C8-Device are shown in Figure 9. It is found that all the spectra for devices are dominated by PL data of P3HT layer [8]. It is seen that devices including Cr atoms exhibit lower PL peak intensity than that of C0-Device, implying that inefficient electron transfer between CdS and P3HT films is achieved for C2-Device, C4-Device, C6-Device and C8-Device [23]. As a consequence, efficient exciton dissociation was succeeded for C0-Device at the interface of CdS/P3HT whereas the other devices display poorer exciton separation at the interface, leading to lower power conversion efficiency for the devices including Cr atoms (will be discussed below).

Table 2. Solar cell parameters of Jsc, Voc, FF and efficiency (Ƞ) of C0, C2, C4, C6 and C8-Device.

Device	J_{sc} (mA.cm^{-2})	V_{oc} (V)	FF	Ƞ (%)
C0-Device	1.670	0.370	0.445	0.296
C2-Device	0.131	0.234	0.261	0.009
C4-Device	0.164	0.823	0.252	0.037
C6-Device	0.246	0.216	0.263	0.015
C8-Device	0.117	0.600	0.256	0.019

Figure 10 shows the current density-voltage characteristics of C2-Device, C4-Device, C6-Device and C8-Device and the inset of Figure 10 indicates the J-V curve of C0-Device for the comparison. In addition, the calculated solar cell parameters are also listed in Table 2. It is observed from Figure 10 and its inset that a remarkable photovoltaic effect is obtained for all the devices. C0-Device exhibits J_{sc} of 1.670 mA/cm^2, V_{oc} of 0.370 V, FF of 0.445 and efficiency of 0.296%, meaning that the highest solar cell efficiency is reached for C0-Device. After Cr-doping of various concentrations, it is seen from Table 2 that all the solar cell parameters deteriorate except for V_{oc} values of C4-Device and C8-Device. It is found that higher V_{oc} scores are achieved for C4-Device and C8-Device as 0.823 V and 0.600 V, respectively compared with that of C0-Device. The improvement in the V_{oc} values for these devices is most probably due to the decline recombination as a consequence of the increased band gap of CdS thin films after Cr-doping as discussed in Figure 6 [23]. On the other hand, particularly, C4-Device displays J_{sc} of 0.164 mA/cm^2, V_{oc} of 0.823 V and FF of 0.252, concluding a PCE of 0.037% that is the highest PCE score within the devices including Cr atoms. With respect to that of C0-Device, it is demonstrated that poorer PCE values of C2-Device, C4-Device, C6-Device and C8-Device are obtained. This reduction in the efficiencies could originate from the following situations: (i) as handled in Figure 1, Cr-doping treatment gets worse the crystal structure of CdS thin films, resulting in the creation of more distorted CdS structure, (ii) as can be seen in Table 1 and Figure 2, the crystalline and grain sizes of C2, C4, C6 and C8 are bigger than that of C0, approving that Cr-doping induces a diminish in the crystalline and grain sizes of the samples. It is well-known that CdS:Cr thin films are preferred to have bigger grains to use them in solar cells as a window layer. However, CdS samples including Cr atoms possess smaller grain size than that of CdS, meaning that poorer PCE values are reached, (iii) as discussed in Figure 7, Cr-doping decreases N3-dye absorption on CdS surface, leading to a worse compatible surface contact between CdS and P3HT

layers, (iv) as argued in Figure 8, Cr-doping causes the increase of PL peak intensity, meaning the formation of more defected CdS structure as a result of the addition of more Cr-atoms in CdS structure and (v) as debated in Figure 10, inefficient exciton dissociation is reached upon Cr-doping, giving rise to less number of free electron-hole pairs that contribute the electrical current.

4. CONCLUSION

CdS:Cr thin films with various amount of Cr atoms from 0 to 8% was prepared by CBD method on ITO-coated glass slides. XRD data showed the cubic growth of all the samples and Cr-doping caused a broadening in the main peak of CdS, meaning the creation of nanocrystalline CdS structure. Decreases in the crystalline and grain sizes of CdS thin films were found upon Cr-doping. Uniform coverage of P3HT films on N3-modified CdS or CdS:Cr surface was succeeded. EDS data demonstrated that a deviation from the stoichiometry was obtained by Cr-doping. More transparent CdS thin films were acquired by 2% and 8% as compared with CdS one. Cr-doping treatment led to a widening of band gap of CdS thin films (from 2.98 eV to 3.36 eV) until 4%, which is most probably by virtue of strong quantum size effect. Further rise of Cr-doping level didn't vary the bandwidth of the CdS samples. The peak intensity of absorption spectrum of C0-Device was higher than those of the others, implying a degradation in the absorbance at the interface of CdS/P3HT was acquired for the devices including Cr atoms. RTPL outputs illustrated an increase in the peak intensity, which means the creation of more defected CdS thin films. PL data of the devices including Cr atoms displayed that a lowering in the peak intensity was seen once Cr atoms were incorporated, suggesting poorer exciton dissociation at CdS/P3HT interface for the devices including Cr atoms. J-V features displayed that C0-Device possessed an efficiency of 0.296% and Cr-doping gave rise to a deterioration in the PCE scores of CdS-based solar cells.

References

[1] A. Uddin, M. Wright. Organic-inorganic hybrid solar cells: A comparative review. Sol. Energy Mater. Sol. Cells 107 (2012) 87-111.

[2] H. Cortina, C. Martínez-Alonso, M. Castillo-Ortega, H. Hu. Cellulose acetate fibers covered by CdS nanoparticles for hybrid solar cell applications. Mater. Sci. Eng. B 177 (2012) 1491-1496.

[3] C.–F. Lin, E.–Z. Liang, S.–M. Shih, W.–F. Su. CdS nanoparticle light-emitting diode on Si. In: Proceedings of Light-Emitting Diodes: Research, Manufacturing, and Applications VI; San Jose, California, United States; 2002. pp. 4641.

[4] R. Demir, S. Okur, M. Şeker. Electrical Characterization of CdS Nanoparticles for Humidity Sensing Applications. Ind. Eng. Chem. Res. 51(8) (2012) 3309-3313.

[5] S. Yılmaz, A. Ünverdi, M. Tomakin, İ. Polat, E. Bacaksız. Surface modification of CBD-grown CdS thin films for hybrid solar cell applications. Optik 185 (2019) 256-263.

[6] S. Yılmaz, M. Tomakin, A. Ünverdi, A. Aboghalon. A Study on Hydrothermal Grown CdS Nanospheres: Effects of Cd/S Molar Ratio. GU J. Sci. 32(4) (2019) 1271-1281.

[7] F. Chen, H. Chen, X. Chen, X. Jiang, W. Qiu, M. Wang, L. Yang. Large-scale fabrication of CdS nanorod arrays on transparent conductive substrates from aqueous solutions. Sol. Energy 85 (2011) 2122-2129.

[8] S. Yılmaz, İ. Polat, M. Tomakin, A. Ünverdi, E. Bacaksız. Enhanced efficiency of CdS/P3HT hybrid solar cells via interfacial modification. Turk. J. Phys. 43 (2019) 116-125.

[9] M.C. Arenas, N. Mendoza, H. Cortina, M.E. Nicho, H. Hu. Influence of poly3-octylthiophene (P3OT) film thickness and preparation method on photovoltaic performance of hybrid ITO/CdS/P3OT/Au solar cells. Sol. Energy Mater. Sol. Cells 94 (2010) 29-33.

[10] A. Nabi, Z. Akhtar, T. Iqbal, A. Ali, M. A. Javid. The electronic and magnetic properties of wurtzite Mn:CdS, Cr:CdS Mn:Cr:CdS: first principles calculations. J. Semicond. 38(7) (2017) 073001-073008.

[11] D. Sharma, B. P. Malik, A. Gaur. Pulsed laser induced optical nonlinearities in undoped, copper doped and chromium doped CdS quantum dots. J. Opt. 17 (2015) 045502-045508.

[12] M. Thambidurai, N. Muthukumarasamy, D. Velauthapillai, N. Murugan, J. Chaudhuri, S. Parameswaran, A. Marathe, S. Agilan, R. Balasundaraprabhu. Effect of Cr-doping on the structural and optical properties of CdS nanoparticles prepared by chemical precipitation method. J. Mater. Sci. Mater. Electron. 23 (2012) 618-624.

[13] K.S. Kumar, A. Divya, P.S. Reddy. Synthesis and characterization of Cr doped CdS nanoparticles stabilized with polyvinylpyrrolidone. Appl. Surf. Sci. 257 (2011) 9515-9518.

[14] P. Srivastava, P. Kumar, K. Singh. Room temperature ferromagnetism in magic-sized Cr-doped CdS diluted magnetic semiconducting quantum dots. J. Nanopart. Res. 13 (2011) 5077-5085.

[15] S. Horoz, O. Sahin. Synthesis, characterizations and photovoltaic properties of Cr-doped CdS QDs. J. Mater. Sci. Mater. Electron. 28 (2017) 17784-17790.

[16] Y. Ren, Z. Zhang, H. Hu, W. Liu. Solvothermal synthesis of Cr-doped MS(M=Zn, Cd) nanostructures with room-temperature ferromagnetic property. Physica E Low Dimens. Syst. Nanostruct. 114 (2019) 113643-113648.

[17] Y.J. Kim, T.K. An, S.J. Oh, D.S. Chung, C.E. Park. Surface modification with MK-2 organic dye in a ZnO/P3HT hybrid solar cell: Impact on device performance. APL Mater. 2 (2014) 076108-076113.

[18] S. Yılmaz, İ. Polat, M. A. Olgar, M. Tomakin, S. B. Töreli, E. Bacaksız. Physical properties of CdS:Ga thin films synthesized by spray pyrolysis

technique. J. Mater. Sci. Mater. Electron. 28 (2017) 3191-3199.

[19] A. Mercy, A.J. Anandhi, K.S. Murugesan, R. Jayavel, R. Kanagadurai, B.M. Boaz. Synthesis, structural and property studies of Ni doped cadmium sulphide quantum dots stabilized in DETA matrix. J. Alloys Compd. 593 (2014) 213-219.

[20] B. Ahmed, A. Kumar Ojha, S. Kumar. One-pot synthesis of Ni doped CdS nanosheets for near infrared emission and excellent photocatalytic materials for degradation of MB dye under UV and sunlight irradiation. Spectrochim. Acta A 179 (2017) 144-154.

[21] S. Yılmaz. The investigation of spray pyrolysis grown CdS thin films doped with flourine atoms. Appl. Surf. Sci. 357(A) (2015) 873-879.

[22] S. Yılmaz, M. Parlak, Ş. Özcan, M. Altunbaş, E. McGlynn, E. Bacaksız. Structural, optical and magnetic properties of Cr doped ZnO microrods prepared by spray pyrolysis method. Appl. Surf. Sci. 257(22) (2011) 9293-9298.

[23] T. Adhikari, U. Jabeen, J.–M. Nunzi, D. Pathak, S.M. Shah. Structural, optical and photovoltaic properties of P3HT and Mn-doped CdS quantum dots based bulk heterojunction hybrid layers. Opt. Mater. 78 (2018) 132-141.